Nuclear Instruments and Methods in Physics Research A 723 (2013) 102–108

Contents lists available at SciVerse ScienceDirect

Nuclear Instruments and Methods in Physics Research A

journal homepage: www.elsevier.com/locate/nima

AstroBox: A novel detection system for very low-energy protons from β-delayed proton decay

E. Pollacco [a], L. Trache [b,c], E. Simmons [b], A. Spiridon [b], M. McCleskey [b], B.T. Roeder [b,*], A. Saastamoinen [b], R.E. Tribble [b], G. Pascovici [c], M. Kebbiri [a], J.P. Mols [a], M. Raillot [a]

[a] IRFU, CEA Saclay, Gif-sur-Yvette, France
[b] Cyclotron Institute, Texas A&M University, College Station, TX 77843-3366, USA
[c] National Institute of Physics and Nuclear Engineering, Bucharest-Magurele, RO-077125, Romania

ARTICLE INFO

Article history:
Received 18 April 2013
Accepted 30 April 2013
Available online 9 May 2013

Keywords:
Micro pattern gas amplifier detector
MPGAD
β-delayed proton decay
^{23}Al
Nuclear astrophysics

ABSTRACT

An instrument, AstroBox, has been developed to perform low energy proton spectroscopy from β-delayed proton emitters of interest to astrophysics studies. Energetic precursor nuclei are identified and stopped in the gas volume of the detector. The subsequent β or β-proton decay traces ionized paths in the gas. The ionization electrons are drifted in an electric field and are amplified with a Micro Pattern Gas Amplifier Detector (MPGAD). The system was tested in-beam using the β-delayed proton-emitter ^{23}Al, which was produced with the p(^{24}Mg,^{23}Al)2n reaction and separated with the Momentum Achromat Recoil Spectrometer (MARS) at the Cyclotron Institute at Texas A&M University. Off-beam proton spectra have essentially no β background down to ~100 keV and have a resolution of ~15 keV (fwhm) for proton-decay lines at $E_p = 197$ and 255 keV. Lines with βp-branching as low as 0.02% are observed. In addition, the device also gives good mass and charge resolution for energetic heavy ions measured in-beam.

1. Introduction: nuclear astrophysics motivation

In many radiative proton capture reactions, X(p, γ)Y, important in steady-state or explosive H-burning in stars or stellar environments, resonant capture dominates the reaction rate. In such cases the reaction rates can be evaluated based on information about the location and strength of the important resonances [1]. This information can be obtained through an indirect method by populating and studying the same metastable states in the compound system Y* through their β-delayed proton decay. β-delayed proton emission (βp) from exotic nuclei was observed to occur in proton-rich nuclei (precursors P), which have sufficiently large *Q*-value to populate the excited states above the proton binding energy in the daughter nucleus Y ($Q_\beta > S_p$) which may decay either by gamma-ray or by proton emission. If the decays are P → Y* → X + p, then the excited states in Y* can be the resonances of interest in the X(p, γ)Y capture if the selection rules for (p, γ) and βp allow for the population of the same states in the compound system Y (energy and spin-parity selection rules). One can determine through proton spectroscopy the energy of the resonances, possible spins and parities, and branching ratios.

This seemingly simple approach is complicated by the fact that the important energy levels for captures in stars are those that lie close to the decay threshold. In phenomena like novae or X-ray bursts (XRB) the temperatures involved are $T = 0.1$–0.4 GK and up to 1 GK, respectively. For these temperatures, the range of energies that contributes most to the reaction rates (the Gamow window) is between 100 and 400 keV for the lower range and up to ~800 keV for the higher range in nuclei around $A = 20$–40. These raise two difficult experimental problems for the observation of very low-energy protons from β-delayed proton decay. The first is related to the need to avoid energy losses of the emitted protons before entering the active area of the detector. To do this, we chose to implant the source in the detector itself. The second is the fact that the lower the energy of the metastable states above the proton threshold, the lower the probability for the proton emission due to the Coulomb barrier and thus gamma-ray emission becomes dominant. To observe very low branching ratios, we need detectors with very high sensitivity. In the case of sources implanted in the detector, that requires a low sensitivity to the β-particles emitted in the first step of the decay process.

Significant success has been achieved [2–4] by implanting the precursor nuclei in thin Si strip detectors, but proton decays with energies below about 300 keV are still dominated by a large continuum background and width widening resulting from the energy loss of the positrons (β^+). We show here how these two problems are solved by using a gas detector. Gas reduces the

* Corresponding author. Tel.: +1 979 845 1411.
E-mail addresses: epollacco@cea.fr (E. Pollacco), broeder@comp.tamu.edu (B.T. Roeder).

0168-9002/$ - see front matter © 2013 Elsevier B.V. All rights reserved.
http://dx.doi.org/10.1016/j.nima.2013.04.084

sensitivity to the β^+ emitted and pushes the background down in energy. A high gain gas amplifier based on a Micro Pattern Gas Amplifier Detector (MPGAD) [5] assures a good gain for proton energy loss while maintaining good resolution. Further we show that AstroBox allows the beam composition to be evaluated per burst.

AstroBox was tested both with sources and with the β-delayed proton decay of ^{23}Al [3,6,7]. Results from the source tests are described in Section 2 and those from the in-beam studies of ^{23}Al decay are given in Section 3. Conclusions are summarized in Section 4.

2. AstroBox

2.1. The AstroBox detector

AstroBox is, basically, a cylindrical gas detector with a few electronic channels. A photograph of the assembly is shown in Fig. 1. A CAD drawing is given in Fig. 2, left panel and a schematic view showing its elements and voltages is given in Fig. 2, right panel. The detector is housed in a stainless steel cylindrical chamber with ports to allow for beam entry through a vacuum tight 50 μm thick Aramica window and for chamber evacuation and gas flow. Two other ports have vacuum tight Kapton windows to allow for X-ray sources to be inserted for calibration. The design of the detector allows for the beam or sources to enter axially or perpendicularly with respect to its symmetry axis. The main components inside the chamber are the cathode, equipotential rings, gating grid (GG), and gas amplifier (MPGAD). Geometrically these elements are stacked and equally spaced. By using the voltages and dimensions given in Fig. 2, right panel, a uniform field is set up in the active volume between the cathode and the gas amplifier. The GG has a grid (100 μm diameter wire with 2 mm pitch) stretched to cover the central area and has a functionality described below. The MPGAD, a Micromegas structure [5], is the main element of AstroBox. It consists of a gold plated anode divided into five areas (Fig. 3, right panel) on a printed-circuit board with an inter-pad spacing of 300 μm. An 18 μm nickel mesh, shown in Fig. 3, left panel, is stretched over the anode and kept at a uniform distance of 128 μm from the anode by placing insulating pods every 5 mm. Amplification of the electrons entering the mesh-pad volume occurs because of the very high electric field strength of approximately 30–40 kV/cm in the 128 μm zone. The manufacture, signal formation and performance of this device are described in detail in [8].

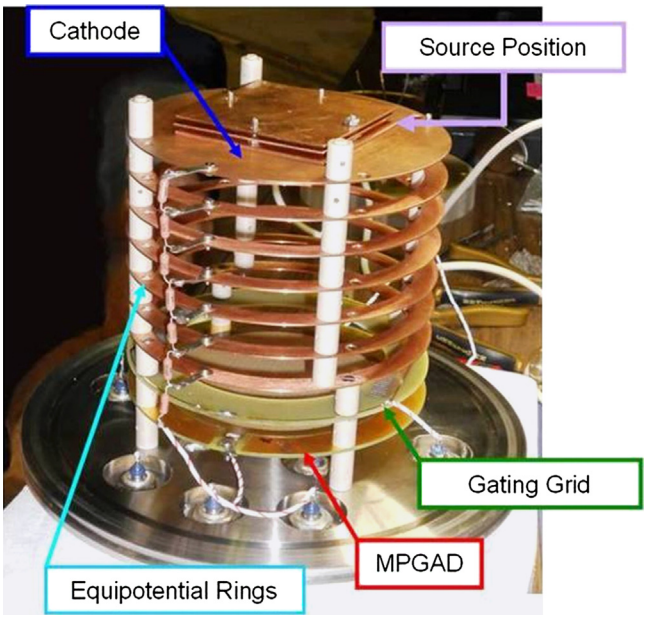

Fig. 1. Picture of AstroBox from the pre-experiment setup. The beam enters perpendicular on cylinder axis.

The gas used was a standard mixture of 90% Ar and 10% methane, P10. A pressure of 800 Torr was selected to ensure that the gas purity remained high in case of leaks. The gas was continuously refreshed at a rate of about 8.5 L/h. The density of the gas was monitored and observed to vary less than 0.1% during operation. The gas handling system is based on a MKS πPC pressure controller unit [9]. The choice of materials employed and the design were chosen to minimize possible contamination of the gas from low vapor pressure material or trapped gases. A clean environment was ensured by flowing the P10 through the assembly for two days prior to use.

Stable bias voltage for the mesh and anode pads was provided from an Ortec Quad Bias Supply 710 and from two Ortec 549 (0–5 kV) bias supply units for the cathode and the GG [10]. Filtering of the bias input to detectors was employed. Signals from the anode pads were fed into 142a/b Ortec pre-amplifiers followed by a classical fast-slow set-up. The trigger was given by signals firing a leading edge discriminator on the central pad. The ADCs from all channels were read following a trigger. For the tests shown here, three electronic chains were set-up and hence the four sector pads were summed into two channels, S1 and S2. The cathode was biased at a fixed negative voltage of 1.8 kV to give an electron drift velocity of ~5 cm/μs.

The functionality of AstroBox is similar to that of a Time-Projection Chamber (TPC), where electrons from the ionization of the gas created by particles losing energy in the active volume drift towards the GG and then onto the gas amplifier. By placing

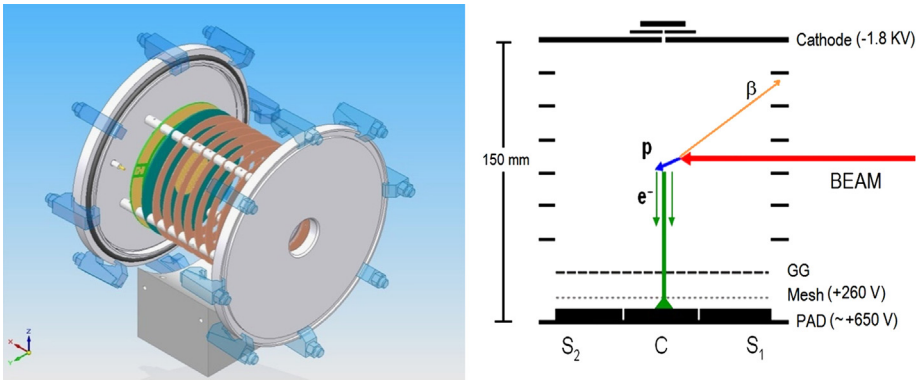

Fig. 2. Left panel: schematic drawing of AstroBox. Right panel: schematic representation of the detector and how it works. The MPGAD Pad is at the bottom.

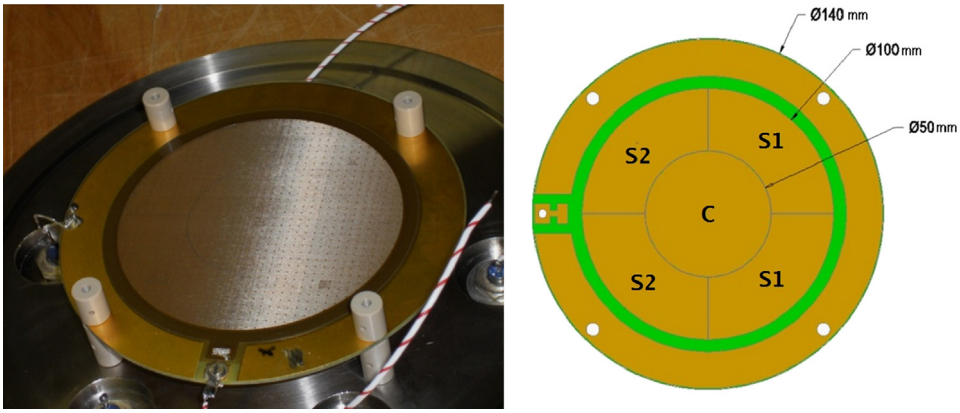

Fig. 3. Left panel: picture of the micromesh sitting on top of the anode. Right panel: schematic drawing of the anode pads.

appropriate bias on the GG, the drifted electrons are collected or partially collected on the MPGAD. For close to 100% transmission of the drifted electrons the grid is set at 0 V. The GG is opaque to electrons at +200 V.

The energy loss in the active gas volume from the stopping beam may be very high (>50 MeV) compared to the required dynamic range (50–4000 keV) to measure the low energy protons. Hence a large number of electrons could reach the anode when the beam enters and stops in AstroBox. To avoid spark damage to the MPGAD, the beam is pulsed with beam-on for implantation and beam-off for the proton measurement. The GG voltage is synchronized with the beam to remove a large fraction of the electrons when the beam is on and be transparent when the beam is off. To do this, a simple but effective circuit was devised for this function. Rise and decay time of the GG are typically 300 μs. By adjusting the GG bias, we could get the system to detect both the beam and the high-energy part of the proton spectrum during the beam-on period. This is particularly useful for beam particle counting and identification and hence normalization, as described in Section 3.2.

2.2. Simulations of the implantation and detector response

Detailed Monte Carlo simulations of the AstroBox detector were carried out prior to the construction of the detector to study how it would function in a typical experiment. These simulations were conducted with the GEANT4 toolkit [11] using the standard packages for the energy loss of charged particles and a custom physics model to generate the β-delayed proton decay of our test case, ^{23}Al. Two important aspects of the test experiment were studied: (1) the implantation of the high energy ^{23}Al ions into the AstroBox chamber and (2) the expected response of the detector for detection of positrons vs. protons during the ^{23}Al decay while the beam was off.

For the simulations of the ^{23}Al ion implantation, it was assumed that the ^{23}Al ions are produced in the manner described in Section 3.1. Thus, the calculations were carried out assuming that a secondary beam of 40 MeV/u ^{23}Al ions with momentum distribution $\Delta p/p = \pm 0.25\%$ that passes through an Al degrader, a 50 μm Aramica window, and finally into the detector chamber itself with P10 gas. The angle of the Al degrader with respect to the incident beam was adjusted such that the ^{23}Al ions are stopped close to the center of the AstroBox active volume. The beam enters AstroBox perpendicular to the electric field. The resulting distribution of the stopped ions along the central axis of the detector is shown in Fig. 4. The simulation showed that it is possible to stop approximately 85% of the ions inside the active gas volume associated with the central pad of the MPGAD. The main contributions to the width of the distribution were shown to be the

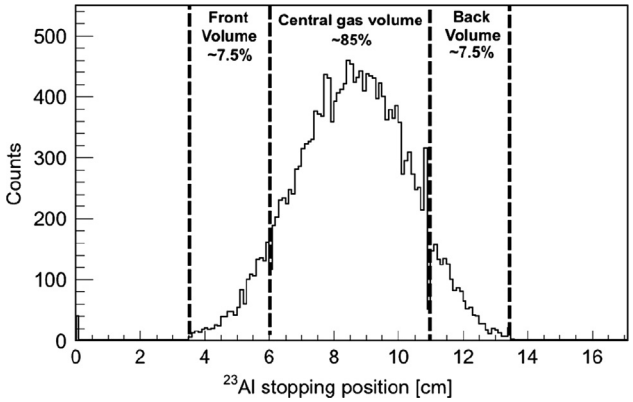

Fig. 4. Monte Carlo simulation of the distribution of the ^{23}Al ions inside AstroBox.

initial momentum spread of the beam and the energy straggling of the ions as they pass through the Al degrader, the entrance window and the gas. As a function of time, the ^{23}Al distribution width is increased slightly due to Brownian motion [12,13]. From known physical chemistry [14,15] of the Argon+CH_4 components of the P10 gas, we estimate that this spread contributes approximately 0.8% to the width of the distribution within the gas for ^{23}Al over ~1 s measurement time in typical operating conditions of the Astrobox.

For the simulations of the AstroBox detector response to the positrons and protons from ^{23}Al decay, separate calculations were carried out. In this case, the ^{23}Al ions were placed inside AstroBox with the distribution as described above. Then, the ^{23}Al nuclei were allowed to decay at random positions given by the distribution. The result of this simulation is shown in Fig. 12 (Section 3.3). The calculations show that the maximum energy deposited by the positrons in central active gas volume is ~150 keV, with most of the positrons depositing less. The calculations also showed that the protons from ^{23}Al decay with energies between 200 and 300 keV should be clearly visible and well-separated from the positron background. This represents a substantial improvement over the previous measurements with implantation into silicon detectors where careful background subtraction was needed [3]. The simulations use recent available proton decay data [3,16] as extracted from the studies with thin Si detectors.

The detection efficiency of AstroBox for protons of various energies was also estimated with the simulation. The efficiency depended on the energy of the protons, the gas type and pressure used, and the size of the expected distribution after the implantation. The variation with energy is shown in Fig. 5. As the entire ^{23}Al distribution fits within the sum of the inner and outer active

volumes, the proton detection efficiency is close to 100% for proton energies below ~1000 keV for triggers with the central pad. Beyond 1000 keV, the path length of the protons in the gas is greater than 2 cm, allowing some of the protons to exit the active gas volumes of the detector and thus reduces the efficiency. This effect is more pronounced if only the central active gas volume is considered. In this case for total energy recovery the efficiency is limited to ~84% at low energy and decays rapidly to zero above 1000 keV. This reflects that the path length of the protons is larger than the diameter of the central volume. The efficiency can be improved by increasing the gas pressure or by using heavier gases at the cost of also increasing the contributions of the positrons to the energy loss spectrum.

2.3. Tests with sources

To establish the functionality of AstroBox, an ^{55}Fe X-ray source and mixed-α source were employed. The ^{55}Fe source viewed the active volume through one of the side ports having a Kapton window. A typical spectrum for the ^{55}Fe source from the central pad is given in Fig. 6, left panel and shows that the resolution for the 5.9 keV peak after subtraction of the 6.5 keV peak is 11% (FWHM). The escape peak at 3 keV is clearly seen. Amplification gain for such spectra was typically of the order of 10^4. The mixed-α source was a mixture of ^{148}Gd, ^{239}Pu, ^{241}Am and ^{244}Cm isotopes covering a range between 3.2 and 5.8 MeV alphas. Tests with this source were performed with gains typically of the order of 20–100. The spectrum from this source is given in Fig. 6, right panel. The typical energy resolution is 2.5% (FWHM) for the ^{241}Am α-line at 5.5 MeV. The observed integrated non-linearity over the 2.6 MeV range of the mixed-α source is less than 1%.

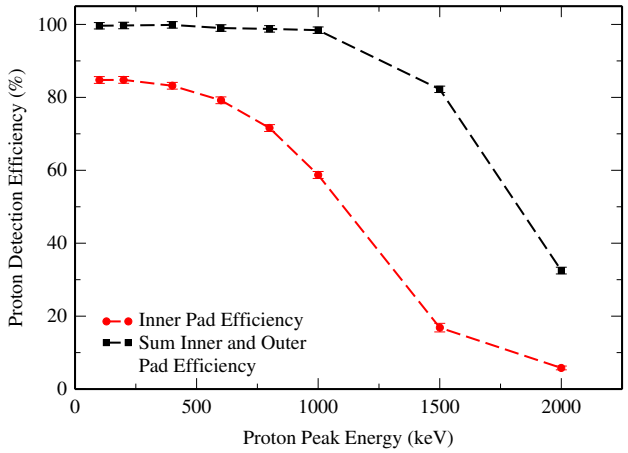

Fig. 5. Simulated proton detection efficiency as a function of energy in AstroBox with the initial ion distribution given in Fig. 4.

3. In-beam tests

3.1. Production and separation of ^{23}Al

The in-beam tests of the AstroBox were done at the Cyclotron Institute at Texas A&M University. A primary beam of ^{24}Mg at 45 MeV/nucleon was generated from the K500 superconducting cyclotron. It impinged on a hydrogen target at 77 K (liquid N_2) temperature and pressure=2 atm. The Momentum Achromat Recoil Spectrometer (MARS) [17] was used to separate a secondary beam of ^{23}Al at 40 MeV/u up to 4000 pps intensity (at $\Delta p/p = \pm 0.6\%$) and 90% purity. The procedure and the resulting parameters were similar to those described in [18]. The ^{23}Al was employed because of its astrophysical significance and because it was previously studied with MARS [3]. Following the results from that study, there were still particular questions about the low-energy region below $E_p = 400$ keV, which is exactly the region of interest for nuclear astrophysics. The major difficulty when using a DSSD is the large background at low energies due to betas ref. [3, Fig. 7] . Further ^{23}Al has reasonably large (1.26%) total proton branchings from β decay with two easily recognizable proton lines at $E_p = 554(8)$ and 828(8) keV that are also in a domain where AstroBox has a good efficiency. Note that the energies and errors given for these proton lines are the proton lab energies given in the most recent measurement with silicon detectors [16].

Attached to the MARS focal plane chamber was a degrader chamber, followed by AstroBox separated by the Aramica window. The degrader chamber contained a rotatable Al foil 625 μm thick, in vacuum. By adjusting the angle of the degrader foil with respect to the beam, the energy of the resulting beam was degraded from 40 MeV/nucleon so that the ^{23}Al stopped above the central pad in AstroBox. In order to implant the nuclei in the center region (the active volume) the angle of the rotating energy degrader angle was fine tuned. During the experiment, the system was operated in two modes: (a) an "implantation-control mode" and (b) "βp measurement mode". In mode (a), the MPGAD gain was adjusted for a dynamic range to be able to measure the energy losses of the heavy ions in the gas (up to 100 MeV total). The beam was not pulsed in this mode. In mode (b), the beam from the cyclotron was pulsed, with the beam on during the 1 s implantation time and the beam off for another 1 s. Before collecting decay data, a delay of about 7 ms was set to ensure that no charge from beam particles was counted. In this time period, the GG was lowered from full opacity to completely transparent. For the measurement of β-delayed protons, the voltage on the mesh and pads was tuned

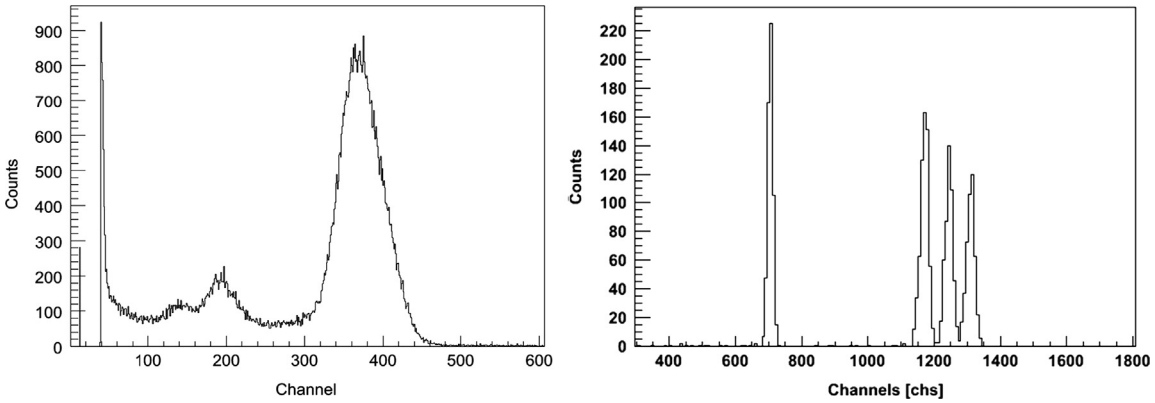

Fig. 6. Left panel: spectrum with the 5.9 keV X-ray peak from an ^{55}Fe source. Right panel: spectrum with the multi-peak α-source with E_α=3.2–5.8 MeV.

such that the detector dynamic range was 0–4 MeV to reach optimum charge resolution. The data channels were closed for 7 ms before the beam came back. The choice of 7 ms is associated with perturbation of the amplifiers during the GG tension changes.

3.2. Detector response to heavy ions

While the principle goal was to study the low energy protons, it is important to identify the beam composition stopping or traversing the active volume and count the number of injected nuclei during implantation (mode b). In order to investigate these capabilities, the detector response to energetic heavy ions was studied. Thus, the secondary beam in AstroBox was set with MARS magnetic parameters such that a cocktail beam was produced by widening the admittance slits at the front of MARS, and widening the final selection slits. The momentum slits of MARS were kept narrow, at ± 0.4 cm, to reach a momentum acceptance of $\Delta p/p = \pm 0.25\%$, and corresponding to a decrease of the rate to ~800 pps. A cocktail of eight different ion species (Z=4–13) with different energies and very different relative intensities was delivered. The composition of the beam cocktail is shown in Fig. 7, as measured with a position sensitive Si strip detector at the MARS focal plane. Once this measurement was completed, the Si strip detector was moved out of the path of the beam to expose AstroBox. The S1 (two entrance quarters connected), center C, and S2 (two exit quarters connected) signals gave a two ΔE–E detector setup. A plot of S2 vs. C is shown in Fig. 8. A similar figure was obtained for S1 vs. C. With the Al degrader foil normal to the beam, the ions pass through the detector and the signals registered correspond to energy losses in the gas. A clear separation of all components of the beam is obtained. The ^{22}Mg and ^{23}Al are well separated in spite of a ratio of 1:100 for their intensities. The resolution is 6% (FWHM) for the energy loss of ^{23}Al in the P10 extracted from projections of Fig. 8. The extracted value from Fig. 7 is 3%. The quoted percentage is not corrected for the resolution of the secondary beam, the straggling and the non-uniformities of the Al degrader foil and in the gas before entering the active volume of the detector, as well as the different path lengths inside the volumes covered by the pads, due to their circular geometry. Also, no effort was made to tune the GG and mesh voltages to improve the resolution. Of interest is that the detector collected charge as a function of calculated energy loss is found to be linear as shown in Fig. 9. The energy losses were evaluated with the code SRIM [19] using the known thickness and angle of the degrader, of the window, the geometry of the pads and the composition and pressure of the gas in the detector. The plot shows no strong evidence for important non-linearity due to high charge density and related effects.

In the implantation control mode, by rotating the Al energy degrader the ^{23}Al nuclei were slowed down so as to be stopped in the center of the detector. This is achieved by inspecting the plots of energy loss in the center pad vs. energy loss in S1 and S2 and performing successive adjustment of the degrader angle.

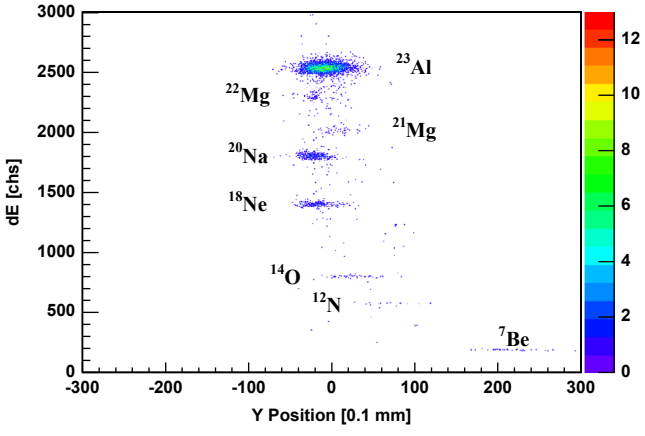

Fig. 7. The isotopes as separated at the focal plane of MARS. The two-dimensional spectrum shown is energy loss vs. position in the Si strip detector.

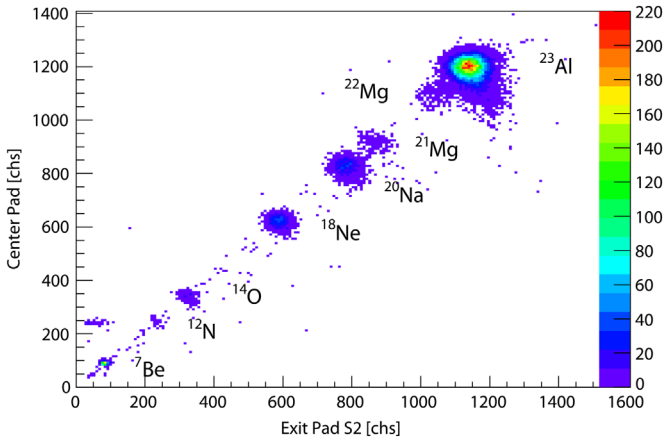

Fig. 8. Two-dimensional plot of the energy loss in the center vs. the exit pad of AstroBox. The particles species are identified by comparison with the spectrum from Fig. 7 and their relative intensities.

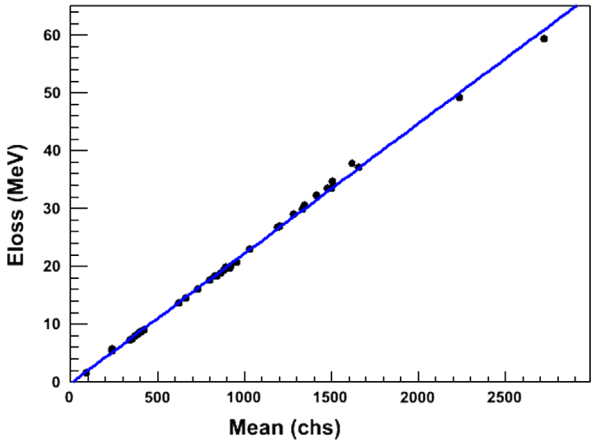

Fig. 9. AstroBox response to the energy deposited by various ions in S_1 (the entrance pad).

In Fig. 10, the two dimensional spectrum of the energy loss in the center pad vs. the energy loss in the entrance pads is given. Most of the ^{23}Al beam is stopped in the detector volume on top of the center pad (as identified by the top band in Fig. 10), while the lower Z impurities (of the same magnetic rigidity) are punching through into the regions covered by the exit pads. Some ^{23}Al stop in the entrance pads (seen on the y-axis of Fig. 10) and some are stopping in the exit pads or punching through the detector (shown on the main diagonal of Fig. 10). The fraction of ^{23}Al not stopped above the center pad amounts to 16%, in agreement with the results of the simulations.

Once the degrader angle was determined, the system was set for the "βp measurement mode". The beam from the cyclotron was pulsed and measurements were only made with beam-off. The detector voltages were adjusted as given above for protons.

3.3. Analysis and results for the β-delayed protons

In the present ^{23}Al case, only β-delayed gamma decay and β-delayed proton decay are possible. Therefore, particle identification is not required. The decay spectra measured in each pad are proton spectra with distortions from the accompanying betas. The spectra obtained can be of three categories. There are events

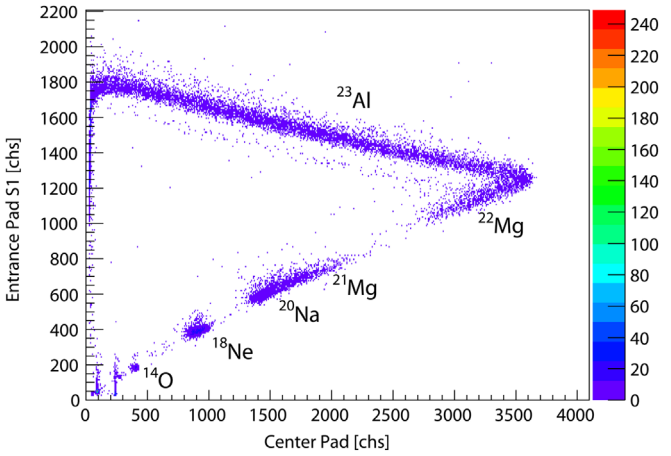

Fig. 10. Implantation control ΔE–E plot at the optimum degrader angle. Ions with $Z<13$ trace the diagonal and punch through the gas volume of the detector. The top band, labeled by ^{23}Al, represents the nuclei stopping in the central volume of the detector at different positions. Events from nuclei stopping before the central gas volume of the detector are shown along the y-axis of this plot.

where the projected proton track is contained within the central pad C and trigger only it, events which trigger only the side pads, S_1 or S_2, and events where the track is shared between the central pad and the one of the surrounding pads, C–S_1 or C–S_2. Events S_1 or S_2, as well as S_2–S_1 type events are not discussed herein. The division between the event classes is imprecise because it depends upon the intrinsic detection characteristic (transverse dispersion of the gas, inter-pad, cross-talk, etc.) and detection thresholds. Electronic thresholds were set as low as about 30 keV.

A proton spectrum is given in Fig. 11, top panel, as detected by the center pad with an anti-coincidence condition with the outer S_1 and S_2 pads. The collection time was 2 h with 500 Hz of ^{23}Al. The spectrum was calibrated employing a pulser and the peaks at 554 and 828 keV [3,16]. From the energy calibration the error in the peak position of the 255 keV peak is 11 keV and consistent with errors evaluated in [3,16]. At low energy, the 197 keV peak is well separated with a peak to background ratio of 3:1. The line shape effects are not asymmetric and hence weakly distorted by the accompanying β^+ ionization of the gas and the threshold effects. For the 255, 554 and 828 keV peaks, the resolution is of the order of 7% (FWHM). Of particular interest is the β^+ background at the level of 200 keV, which is reduced by a factor of ~100 with respect to [3]. The background drops at a level comparable to the height of the proton peak at 197 keV for a beta energy loss around 100 keV. In Fig. 11, bottom panel, the C–S_1 is given and shows the linear sharing of the track energy between C and S_1. A similar 2-D spectrum for C–S_2 is available. Again, the calibration of the S_1 and S_2 spectra utilizes the known peaks for ^{23}Al [3,16] and the pulser.

It is to be noted that the calibration lines from α and X-ray sources are too far away in energy and were not used in this work to verify the calibration. Also the resolution as a function of proton energy should be governed by the stochastic effects and hence should vary like $E_p^{-1/2}$. We note that in comparing calibration runs with ^{55}Fe and α-emitting sources as well as beam data this relationship does not hold. The proton width data can be approximated with a parameterization of 2.35σ (FWHM) $= 180E_p^{-1/2}$ keV. Further statistics and analysis will be published in a later paper. It should be noted that the present system gives the energy resolution measures for MPGAD devices at low 200–300 keV proton energies.

The proton spectrum given in Fig. 11 is compared with GEANT4 simulations in Fig. 12. It assumes the published peak positions [3,16] and branching with the experimental and software constrains given above. The comparison shows that the spectrum is

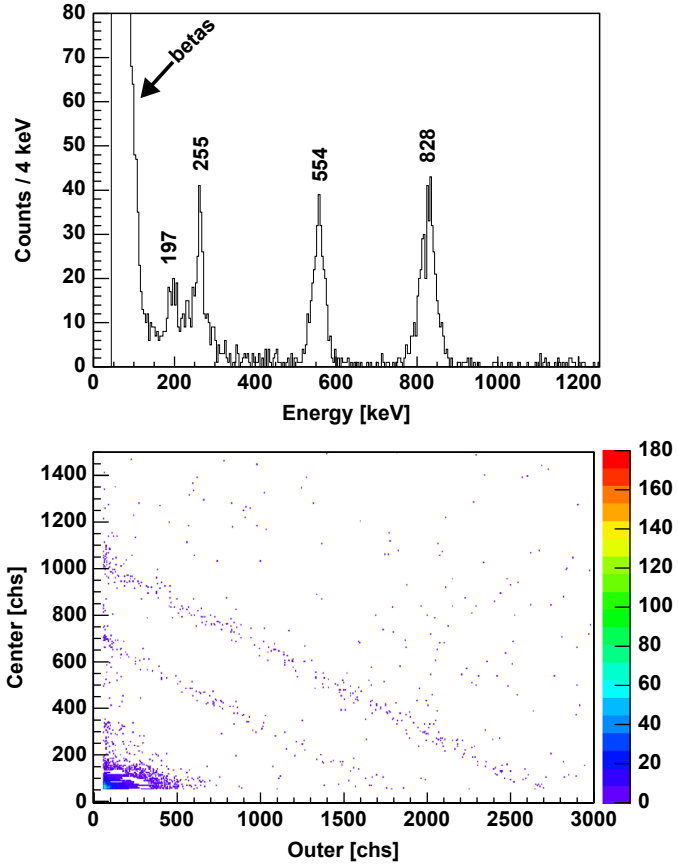

Fig. 11. Top panel: spectrum obtained from the anticoincidence of the center with the outer pad. Energies of the proton peaks shown are the proton lab energies given in [16]. Bottom panel: the center pad vs. the outer pad for the same data.

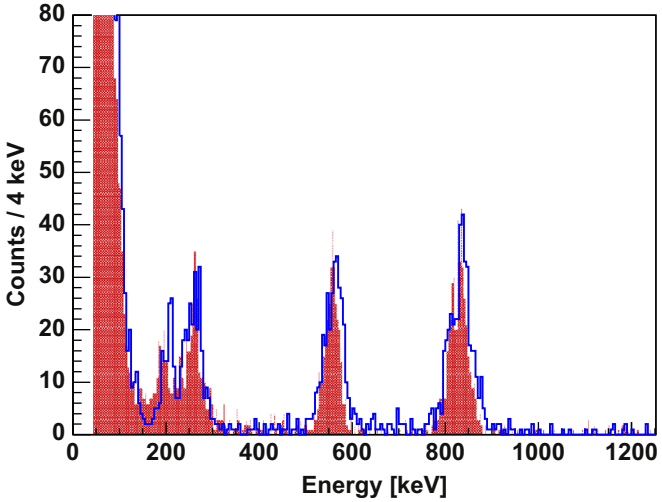

Fig. 12. Overlay of the ^{23}Al proton decay data with the GEANT4 simulation. The data are shown in the red shading and the simulation is shown by the blue line. (For interpretation of the references to color in this figure caption, the reader is referred to the web version of this article.)

well reproduced by the simulations in the peak position, line shape and relative peak intensities. We conclude that the simulation is reproducing the distribution of ions in the detector, the corresponding absolute efficiencies (see Section 2.2) and the ionization processes taking place in the detector. Further, the simulation describes the low charge deposit by the positrons as measured experimentally very well.

In this article, we will not quote measured absolute efficiencies. However it is to be noted that it is quite feasible to count the number of incident species by beam burst and the following proton yield as a function of beam counts. Along with corrections via the simulation, this will yield the absolute branching ratios. This work is in progress and values will be given in a future publication.

4. Conclusions

A gas detector employing a MPGAD, AstroBox, has been built to measure very-low energy protons from β-delayed proton emitters of interest to nuclear astrophysics. To evaluate the performance of AstroBox, a secondary beam of ^{23}Al at 40 MeV/u was produced, separated and then implanted in the gas volume of the detector in test measurements. A large reduction in the β^+ background in the proton spectra was obtained, allowing the measurement of proton peaks as low as $E_p = 200$ keV with 7% (FWHM) resolution and giving estimated βp-branching as low as 0.02%. This excellent performance is due to a combination of four factors:

1. The exotic nuclei are implanted inside the detector itself (no windows or dead layers for the protons emitted).
2. Gas is used as the detection medium (low sensitivity to positrons and gammas).
3. A MPGAD is used to ensure a high amplification factor yielding good charge resolution.
4. Detector components that allow for the implanted beam to be analyzed and counted burst-by-burst.

Further, simulations based on GEANT4 coupled with data show that the processes in the charge production are well understood and that very-high efficiencies are expected, while the detector allows us to record low proton energies from βp, it is efficient only in a relatively narrow regime of energies (100–1000 keV). Hence as it stands, it is a not a universal tool for proton decay studies, but it is an excellent tool for the observation of the very low energy range relevant for the study of resonances of interest in nuclear astrophysics. Simulations have been undertaken to optimise larger gas volumes and employing heavier gases at higher pressures to investigate the capabilities of this detector for measuring higher energy protons. These will be employed in near future experiments. Better results on the background and resolution are expected for the new configurations. Further, multi-channel devices covering large volumes (ACTAR-TPC [20]) and in a magnetic field (AT-TPC [21], SAMURAI-TPC [22]) will be employed in future facilities. Hence, we anticipate that the technique suggested herein will be extended to cover to a full range of resonant spectroscopy for radiative proton and α capture reactions of importance in nuclear astrophysics.

In this paper, we also show that instrumentation can be developed with promising performances for slow heavy ions that would deposit 10–100 MeV. Thus, the technique could be employed to develop a good energy loss detector that would be valuable in particle identification schemes (focal plane detectors, beam trackers, etc.). The instrument is straight forward to build with few electronic channels, radiation hard, and resilient in its use.

Acknowledgment

This work was supported by the U.S. Department of Energy under Grant nos. DE-FG02-93ER40773 and DE-FG52-09NA29467.

References

[1] C.E. Rolfs, W.S. Rodney, Cauldrons in the Cosmos: Nuclear Astrophysics, University of Chicago Press, Chicago, 2005.
[2] L. Trache, et al., PoS (NIC X), in: Proceedings of 10th Symposium on Nuclei in the Cosmos, July 27–August 1, 2008, Mackinac Island, MI, vol. 163, 2008.
[3] A. Saastamoinen, et al., Physical Review C 83 (2011) 045808.
[4] M. McCleskey, et al., Nuclear Instruments and Methods in Physics Research Section A 700 (2013) 124.
[5] Y. Giomataris, Ph. Rebourgeard, J.P. Robert, G. Charpak, Nuclear Instruments and Methods in Physics Research Section A 376 (1996) 29.
[6] L. Trache, et al., Proceedings of International Conference on Nuclear Physics for Astrophysics V, April 3–8, 2011, Eilat, Israel.; L. Trache et al., in: Proceedings of Fourth International Conference on Proton-emitting Nuclei (PROCON2011), B. Blank (Ed.), AIP Conference Proceedings Series, Bordeaux, France, June 6–10, 2011, vol. 1409, Melville, NY, 2011.
[7] A. Spiridon, PoS (ENAS 6) 039, in: Proceedings of 6th European School on Experimental Nuclear Astrophysics, 2011.
[8] I. Giomataris, et al., Nuclear Instruments and Methods in Physics Research Section A 560 (2006) 405.
[9] MKS Instruments, Andover, MA, USA, ⟨www.mksinst.com⟩.
[10] ORTEC, Oak Ridge, TN, USA, ⟨www.ortec-online.com/Solutions/modular-electronic-instruments.aspx⟩.
[11] S. Agostinelli, et al., Nuclear Instruments and Methods in Physics Research Section A 506 (2003) 250.
[12] A. Einstein, Annals of Physics 17 (1905) 549.
[13] P. Langevin, Comptes Rendus de l'Académie des Sciences (Paris) 146 (1908) 530.
[14] A.B. Rakshit, C.S. Roy, A.K. Barua, Journal of Chemical Physics 59 (1973) 3633.
[15] E. May, R.F. Berg, M.R. Moldover, International Journal of Thermophysics 28 (2007) 1085.
[16] O.S. Kirsebom, H.O.U. Fynbo, A. Jokinen, M. Mardurga, K. Riisager, A. Saastamoinen, O. Tengblad, J. Aysto, The European Physical Journal A 47 (2011) 130.
[17] R.E. Tribble, R.H. Burch, C.A. Gagliardi, Nuclear Instruments and Methods in Physics Section A 285 (1989) 441.
[18] V.E. Iacob, Y. Zhai, T. Al-Abdullah, C. Fu, J.C. Hardy, N. Nica, H.I. Park, G. Tabacaru, L. Trache, R.E. Tribble, Physical Review C 74 (2006) 045810.
[19] J.F. Ziegler, J.P. Biersack, M.D. Ziegler, SRIM—The Stopping and Range of Ions in Matter, SRIM Co., 2008, ISBN 0-9654207-1-X, ⟨www.srim.org⟩.
[20] ACTAR-TPC, ⟨http://pro.ganil-spiral2.eu/spiral2/instrumentation/actar-tpc⟩.
[21] AT-TPC, ⟨http://www.nscl.msu.edu/exp/sr/attpc⟩.
[22] SAMURAI-TPC, ⟨https://groups.nscl.msu.edu/hira/sep.htm⟩.